

An Adaptive Parameter Estimation for Guided Filter based Image Deconvolution

Hang Yang, Zhongbo Zhang, and Yujing Guan

Abstract—Image deconvolution is still to be a challenging ill-posed problem for recovering a clear image from a given blurry image, when the point spread function is known. Although competitive deconvolution methods are numerically impressive and approach theoretical limits, they are becoming more complex, making analysis, and implementation difficult. Furthermore, accurate estimation of the regularization parameter is not easy for successfully solving image deconvolution problems. In this paper, we develop an effective approach for image restoration based on one explicit image filter - guided filter. By applying the decouple of denoising and deblurring techniques to the deconvolution model, we reduce the optimization complexity and achieve a simple but effective algorithm to automatically compute the parameter in each iteration, which is based on Morozov's discrepancy principle. Experimental results demonstrate that the proposed algorithm outperforms many state-of-the-art deconvolution methods in terms of both ISNR and visual quality.

Keywords—Image deconvolution, guided filter, edge-preserving, adaptive parameter estimation.

I. INTRODUCTION

IMAGE deconvolution is a classical inverse problem existing in the field of computer vision and image processing[1]. For instance, the image might be captured during the time when the camera is moved, in which case the image is corrupted by motion blur. Image restoration becomes necessary, which aims at estimating the original scene from the blurred and noisy observation, and it is one of the most important operations for future processing.

Mathematically, the model of degradation processing is often written as the convolution of the original image with a low-pass filter

$$g = \mathcal{H}u_{orig} + \gamma = h * u_{orig} + \gamma \quad (1)$$

where u_{orig} and g are the clear image and the observed image, respectively. γ is zero-mean additive white Gaussian noise with variance σ^2 . h is the point spread function (PSF) of a linear time-invariant (LTI) system \mathcal{H} , and $*$ denotes convolution.

The inversion of the blurring is an ill-condition problem, even though the blur kernel h is known, restoring coherent high frequency image details remains be very difficult[2].

It can broadly divide into two classes of image deconvolution methods. The first class comprises of regularized inversion

followed by image denoising, and the second class estimates the desired image based on a variational optimization problem with some regularity conditions.

The methods of first class apply a regularized inversion of the blur, followed by a denoising approach. In the first step, the inversion of the blur is performed in Fourier domain. This makes the image sharper, but also has the effect of amplifying the noise, as well as creating correlations in the noise[3]. Then, a powerful denoising method is used to remove leaked noise and artifacts. Many image denoising algorithms have been employed for this task: for example, multiresolution transform based method [4], [5], the shape adaptive discrete cosine transform (SA-DCT)[7], the Gaussian scale mixture model (GSM) [6], and the block matching with 3D-filtering(BM3D) [8].

The Total variation (TV) model[9], [10], L_0 -ABS[11], and SURE-LET[12] belong to the second category. The TV model assumes that the l_1 -norm of the clear image's gradient is small. It is well known for its edge-preserving property. Many algorithms based on this model have been proposed in [10],[13],[14]. L_0 -ABS[11] is a sparsity-based deconvolution method exploiting a fixed transform. SURE-LET[12] method uses the minimization of a regularized SURE (*Steins* unbiased risk estimate) for designing deblurring method expressed as a linear expansion of thresholds. It has also shown that edge-preserving filter based restoration algorithms can also obtain good results in Refs [15], [16].

In recent years, the self-similarity and the sparsity of images are usually integrated to obtain better performance [17], [18], [19], [20]. In [17], the cost function of image deconvolution solution incorporates two regularization terms, which separately characterize self-similarity and sparsity, to improve the image quality. A nonlocally centralized sparse representation (NCSR) method is proposed in [18], it centralizes the sparse coding coefficients of the blurred image to enhance the performance of image deconvolution. Low-rank modeling based methods have also achieved great success in image deconvolution[23], [24], [25]. Since the property of image nonlocal self-similarity, similar patches are grouped in a low-rank matrix, then the matrix completion is performed each patch group to recover the image.

The computation of the regularization parameter is another essential issue in our deconvolution process. By adjusting regularization parameter, a compromise is achieved to preserve the nature of the restored image and suppress the noise. There are many methods to select the regularization parameter for Tikhonov-regularized problems, however, most algorithms only fix a predetermined regularization parameter for the whole restoration process[9],[26],[27].

This work is supported by the National Science Foundation of China under Grant 61401425. Hang Yang is with Changchun Institute of Optics, Fine Mechanics and Physics, Chinese Academy of Science, Changchun 130033, China. (e-mail: yanghang09@mails.jlu.edu.cn)

Zhongbo Zhang and Yujing Guan are with Jilin University. (e-mail: zhongbozhang@jlu.edu.cn, guanyj@jlu.edu.cn)

Nevertheless, in recent works, a few methods focus on the adaptive parameter selection for the restoration problem. Usually, the parameter is estimated by the trial-and-error approach, for instance, the L-curve method [28], the majorization-minimization (MM) approach [29], the generalized cross-validation (GCV) method [30], the variational Bayesian approach [31], and Morozov’s discrepancy principle [32], [33],

In this work ¹, we propose an efficient patch less approach to image deconvolution problem by exploiting guided filter [37]. Derived from a local linear model, guided filter generates the filtering output by considering the content of a guidance image. We first integrate this filter into an iterative deconvolution algorithm. Our method is consisted by two parts: deblurring and denoising. In the denoising step, two simple cost functions are designed, and the solutions of them are one noisier estimated image and a less noisy one. The former will be filtered as input image and the latter will work as the guidance image respectively in the denoising step. During the denoising process, the guided filter will be utilized to the output of last step to reduce leaked noise and refine the result of last step. Furthermore, the regularization parameter plays an important role in our method, and it is essential for successfully solving ill-posed image deconvolution problems. We apply the Morozov’s discrepancy principle to automatically compute regularization parameter at each iteration. Experiments manifest that our algorithm is effective on finding a good regularization parameter, and the proposed algorithm outperforms many competitive methods in both ISNR and visual quality.

This paper is organized as follows. A brief overview of the guided filter is given in Section II. Section III shows how the guided filter is applied to regularize the deconvolution problem and how the regularization parameter is updated. Simulation results and the effectiveness of choosing regularization parameter are given in Section IV. Finally, a succinct conclusion is drawn in Section V.

II. GUIDED IMAGE FILTERING

Recently, the technique for edge-perserving filtering has been a popular research topic in computer vision and image processing[34]. Edge-aware filters such as bilateral filter [35], and L0 smooth filter [36] can suppress noise while preserving important structures. The guided filter [37][38] is one of the fastest algorithms for edge-preserving filters, and it is easy to implement. In this paper, the guided filter is first applied for image deconvolution.

Now, we introduce guided filter, which involves a filtering input image u_p , an filtering output image u and a guidance image u_I . Both u_I and u_p are given beforehand according to the application, and they can be identical.

The key assumption of the guided filter is a local linear model between the guidance u_I and the filtering output u . It assumes that u is a linear transform of u_I in a window ω_k

centered at the pixel k (the size of ω_k is $w \times w$.):

$$u(i) = a_k u_I(i) + b_k \quad (2)$$

where (a_k, b_k) are some linear coefficients assumed to be constant in ω_k .

To compute the linear coefficients (a_k, b_k) , it needs constraints from the filtering input p . Specifically, one can minimize the following cost function in the window ω_k

$$E(a_k, b_k) = \sum_{i \in \omega_k} ((a_k u_I(i) + b_k - u_p(i))^2 + \varepsilon a_k^2) \quad (3)$$

Here ε is a regularization parameter penalizing large a_k . The solution of Eq.(3) can be written as:

$$a_k = \frac{\frac{1}{w^2} \sum_{i \in \omega_k} u_I(i) u_p(i) - \mu_k \bar{p}_k}{\sigma_k^2 + \varepsilon} \quad (4)$$

$$b_k = \bar{p}_k - a_k \mu_k \quad (5)$$

Here, μ_k and σ_k are the mean and variance of u_I in ω_k , and \bar{p}_k is the mean of u_p in ω_k .

However, a pixel i is involved in all the overlapping windows ω_k that cover i , so the value of $u(i)$ in Eq.(2) is not the same when it is computed in different windows. A native strategy is to average all the possible values of $u(i)$. So, we compute the filtering output by:

$$u(i) = \bar{a}_i u_I(i) + \bar{b}_i \quad (6)$$

where $\bar{a}_i = \frac{1}{w^2} \sum_{k \in \omega_k} a_k$ and $\bar{b}_i = \frac{1}{w^2} \sum_{k \in \omega_k} b_k$ are the average coefficients of all windows overlapping i . More details and analysis can be found in [38].

We denote Eq.(6) as $u = \mathbf{guidfilter}(u_I, u_p)$.

III. ALGORITHM

A. Guided Image Deconvolution

In this proposed method, we plan to restore the blurred image by iteratively Fourier regularization and image smoothing via guided filter(GF). Fig. 1 summarizes the main processes of our image deconvolution method based on guided filtering (GFD). The proposed algorithm relies on two steps: (1) two cost functions are proposed to obtain a filtering input image and a guidance image, (2) a sharp image is estimated using a guided filtering. We will give the detailed description of these two steps in this section.

In this work, we minimize the following cost function to estimate the original image:

$$\min_u \|g - h * u\|^2 + \lambda \|u - \mathbf{GF}(z, u)\|^2 \quad (7)$$

where \mathbf{GF} is the guided filter smoothing operation[37], and z is the guidance image. However, directly solving this problem is difficult because $\mathbf{GF}(\cdot, \cdot)$ is highly nonlinear. So, we found that the decouple of deblurring and denoising steps can achieve a good result in practice.

The deblurring step has the positive effect of localizing information, but it has the negative effect of introducing

¹It is the extension and improvement of the preliminary version presented in ICIP’13 [15]. It is worth mentioning that the work [15] was identified as falling within the top 10% of all accepted manuscripts.

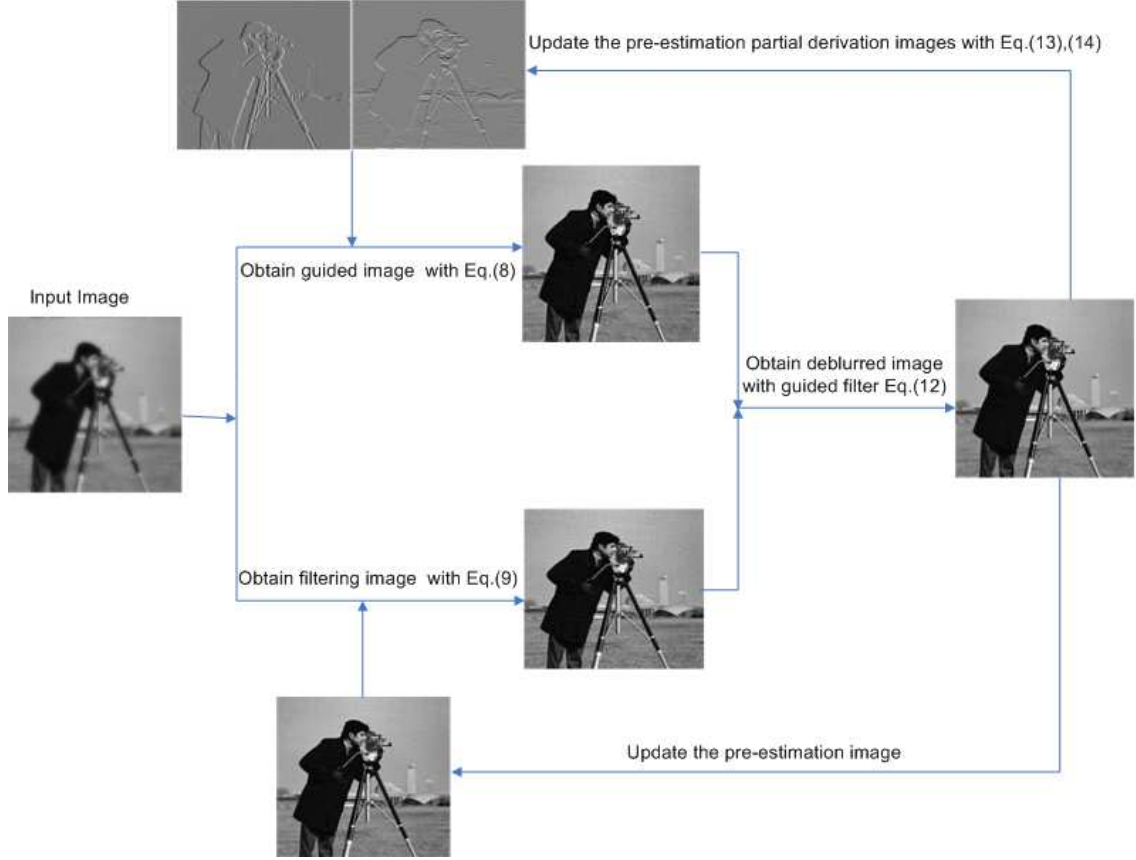


Fig. 1. Schematic diagram of the proposed image deconvolution method.

ringing artifacts. In the **deblurring** step, to obtain a sharper image from the observation, we propose two cost functions:

$$u_I = \arg \min_u \{ \lambda (\| \partial_x u - v_x \|_2^2 + \| \partial_y u - v_y \|_2^2) + \| h * u - g \|_2^2 \} \quad (8)$$

$$u_p = \arg \min_u \{ \lambda \| u - v \|_2^2 + \| h * u - g \|_2^2 \} \quad (9)$$

where $\lambda > 0$ is the regularization parameter, v , v_x and v_y are pre-estimated natural image, partial derivation image in x direction and partial derivation image in y direction, respectively.

Alternatively, we diagonalized derivative operators after Fast Fourier Transform (FFT) for speedup. It can be solved in the

Fourier domain

$$\mathcal{F}(u_I) = \frac{\mathcal{F}(h)^* \cdot \mathcal{F}(g)}{|\mathcal{F}(h)|^2 + \lambda (|\mathcal{F}(\partial_x)|^2 + |\mathcal{F}(\partial_y)|^2)} + \lambda \frac{\mathcal{F}(\partial_x)^* \cdot \mathcal{F}(v_x) + \mathcal{F}(\partial_y)^* \cdot \mathcal{F}(v_y)}{|\mathcal{F}(h)|^2 + \lambda (|\mathcal{F}(\partial_x)|^2 + |\mathcal{F}(\partial_y)|^2)} \quad (10)$$

$$\mathcal{F}(u_p) = \frac{\mathcal{F}(h)^* \cdot \mathcal{F}(g) + \lambda \mathcal{F}(v)}{|\mathcal{F}(h)|^2 + \lambda} \quad (11)$$

where \mathcal{F} denotes the FFT operator and $\mathcal{F}(\cdot)^*$ is the complex conjugate. The plus, multiplication, and division are all component-wise operators.

Solving Eq.(11) yields image u_p that contains useful high-frequency structures and a special form of distortions. In the alternating minimization process, the high-frequency image details are preserved in the denoising step, while the noise in u_p is gradually reduced.

The goal of **denoising** is to suppress the amplified noise and artifacts introduced by Eq.(11), the guided filter is applied to smooth the u_p , and u_I is used as the guidance image. Since the guided filter has shown promising performance, it has

good edge-aware smoothing properties near the edges. Also, it produces distortion free result by removing the gradient reversals artifacts. Moreover, the guided filter considers the intensity information and texture of neighboring pixels in a window. In terms of edge-preserving smoothing, it is useful for removing the artifacts. Therefore in our work, the guided filter is integrated to the deconvolution mode and obtain a reliable sharp image:

$$v = \mathbf{guidfilter}(u_I, u_p) \quad (12)$$

The filtering output v is used as the pre-estimation image in Eq.(9).

After the regularized inversion in Fourier domain [see Eq.(10) and (11)], the image u_p contains more leaked noise and texture details than u_I . So we use u_p as the filtering input image and u_I as the guidance image to reduce the leaked noise and recover some details.

Another problem is how to obtain the pre-estimation image v_x and v_y in Eq.(8). The first term in Eq.(8) uses image derivatives for reducing ringing artifacts. The regularization term $\|\nabla u\|$ prefers u with smooth gradients, as mentioned in [26]. A simple method is $v_x = \partial_x v, v_y = \partial_y v$ which contains not only high-contrast edges but also enhanced noises. In this paper, we remove the noise by using the guided image filter again. Then, we compute the v_x and v_y as follows:

$$v_x = \mathbf{guidfilter}(\partial_x v, \partial_x v) \quad (13)$$

$$v_y = \mathbf{guidfilter}(\partial_y v, \partial_y v) \quad (14)$$

The results can preserve most of the useful information (edges) and ensure spatial consistency of the images, meanwhile suppress the enhanced noise.

The guided filter output is a locally linear transform of the guidance image. This filter has the edge-preserving smoothing property like the bilateral filter, but does not suffer from the gradient reversal artifacts. So we integrate the guided filter into the deconvolution problem, which leads to a powerful method that produces high quality results.

Meanwhile, the guided filter has a fast and non-approximate linear-time operator, whose computational complexity is only depend on the size of image. It has an $O(N^2)$ time (in the number of pixels N^2) exact algorithm for both gray-scale and color images[37].

We summarize the proposed algorithm as follows :

Step 0: Set $k = 0$, pre-estimated image $v^k = v_x^k = v_y^k = 0$.

Step 1: Iterate on $k = 1, 2, \dots, iter$

1.1: Use v^k, v_x^k and v_y^k to obtain the filtering input image u_p^k and the guidance image u_I^k with Eq.(8) and Eq.(9), respectively.

1.2: Apply guided filter to u_p^k with the guidance image u_I^k with Eq.(12), and obtain a filtered output $v^{k+1} = \mathbf{guidfilter}(u_p^k, u_I^k)$.

1.3: Apply guided filter to $\partial_x v^k$ and $\partial_y v^k$ with Eq.(13) and Eq.(14) to obtain v_x^k and v_y^k , respectively, and $k = k + 1$.

Step 2: Output v^{iter} .

For initialization, v^0 is set to be zero (a black image).

B. Choose Regularization Parameter

Note that the Fourier-based regularized inverse operator in Eq.(12) and (13), and the deblurred images depend greatly on the regularization parameter λ . In this subsection, we propose a simple but effective method to estimate the parameter automatically. It depends only on the data and automatically computes the regularization parameter according to the data.

The Morozov's discrepancy principle [39] is useful for the selection of λ when the noise variance is available. Based on this principle, for an image of $N \times N$ size, a good estimation of the deconvolution problem should lie in set

$$S = \{u; \|h * u - g\|_2^2 \leq c\} \quad (15)$$

where $c = \rho N^2 \sigma^2$, and ρ is a predetermined parameter.

Indeed, it does not exist uniform criterion for estimating ρ and it is still a pendent problem deserving further study. For Tikhonov-regularized algorithms, one feasible approach for selecting ρ is the equivalent degrees of freedom (EDF) method[33].

Now, we show how to determine the parameter λ . By Parseval's theorem and Eq.(11)

$$\begin{aligned} \|h * u_p - g\|_2^2 &= \left\| \frac{\lambda(\mathcal{F}(h) \cdot \mathcal{F}(v) - \mathcal{F}(g))}{|\mathcal{F}(h)|^2 + \lambda} \right\|_2^2 \\ &\leq \|h * v - g\|_2^2 \end{aligned} \quad (16)$$

If the pre-estimated image $v \in S$, then $u_p \in S$, so we set $\lambda = \infty, u_I = u_p = v$; else, a proper parameter λ can be computed as follows: in the case when the additive noise variance is available, a proper regularization parameter λ is computed such that the restored image u_p in Eq.(11) satisfies

$$\|h * u_p - g\|_2^2 = \left\| \frac{\lambda(\mathcal{F}(h) \cdot \mathcal{F}(v) - \mathcal{F}(g))}{|\mathcal{F}(h)|^2 + \lambda} \right\|_2^2 = \rho N^2 \sigma^2 \quad (17)$$

One can see that the right-hand side is monotonically increasing function in λ , hence we can determine the unique solution **via bisection**.

In this paper, the noise variance σ^2 is estimated with the wavelet transform based median rule [40]. Once σ^2 is available, $c = \rho N^2 \sigma^2$ is generally used to compute c . $\rho = 1$ had been a common choice. From Eq.(17), it is clear that the λ increases with the increase of ρ . In practice, we find that a large λ ($\rho = 1$) can substantially cut down the noise variance, but it often causes a noisy image with ringing artifacts. So, we should select a smaller λ ($\rho < 1$) which can achieve an edge-aware image with less noise. Then, our effective filtering approach based on guided filter can be employed in the denoising step.

In our opinion, the parameter ρ should satisfy an important property: the ρ should decrease with the increase of image variance. For instance, a smooth image which contains few high-frequency information can not produce the strong ringing effects with large ρ , and a large ρ could substantially suppress the noise. That is to say, the parameter ρ should increase with the decrease of image variance. According to this property, we set ρ as following:

$$\rho = \begin{cases} s^2, & thresh > \tau \\ s, & thresh \leq \tau \end{cases} \quad (18)$$

$$s = 1 - \frac{\|g - \mu(g)\|_2^2 - N^2\sigma^2}{\|g\|_2^2} \quad (19)$$

$$thresh = \sqrt{\frac{\|g - \mu(g)\|_2^2 - N^2\sigma^2}{N^2\sigma^2 \|v - \mu(v)\|_2^2}} \quad (20)$$

where $\mu(g)$ and $\mu(v)$ denote the mean of g and v , respectively.

This method is simple but practical for computing λ , it slightly adjusting the value of λ according to the variance of g . $thresh$ shows the ratio of the variance of g and the variance of v . It means that when v becomes clearer, the variance of v is larger, and the value of $thresh$ is small. So we should increase the λ , because the weight of v is large in Eq.(10) and Eq.(11).

In this work, we suggest setting $\tau = 0.6$ in our experiments and not adjusting the parameters for different types of images. We find that this parameter choosing approach is robust to the extent towards the variations of the image size and the image type. There are some similar strategies in some works dealing with the constrained TV restoration problem [33].

IV. NUMERICAL RESULTS

In this section, some simulation results are conducted to verify the performance of our algorithm for image deconvolution application.

We use the BSNR (blurred signal-to-noise ratio) and the ISNR (improvement in signal-to-noise-ratio) to evaluate the quality of the observed and the restored images, respectively. They are defined as follows:

$$BSNR = 10 \log_{10} Var(g)/N^2\sigma^2 \quad (21)$$

$$ISNR = 10 \log_{10} \left(\frac{\|u_{orig} - g\|_2^2}{\|u_{orig} - \hat{u}\|_2^2} \right) \quad (22)$$

where \hat{u} is the corresponding restored image.

Two 256×256 (*Cameraman* and *House*) and two 512×512 (*Lena* and *Man*) images shown in Fig. 4 are used in the experiments.

A. Experiment 1 – Choice of ρ

In the first experiment, we explain why a suitable upper bound $c = \rho N^2\sigma^2$ for the discrepancy principle is more attractive in image deconvolution. In particular, we demonstrate that the proposed method we derived in Eq.(18) is successful in finding the λ automatically.

The test images are *Cameraman* and *Lena*. The boxcar blur (9×9) and the Gaussian blur (25×25 with std = 1.6) are used in this experiment. There are many previous methods[11][8] for image deconvolution problem have shown the ISNR performance for these two point spread functions. We add a Gaussian noise to each blurred image such that the BSNRs of the observed images are 20, 30, and 40 dB, respectively.

The changes of ISNR against ρ is shown in Fig.1. The ISNRs obtained by our choice of given in Eq.(18) are marked by "•" and those obtained by the conventional setting of $\rho = 1$ are marked by "◇". It is clearly shown that, the ISNRs obtained by our approach are always close to the maximum. However, for $\rho = 1$, its ISNRs are far from the maximum.



Fig. 2. *Cameraman*(256×256),*House*(256×256),*Lena*(512×512),*Man*(512×512).

B. Experiment 2 – Comparison with the State-of-the-Art

In this subsection, we compare the proposed algorithm with five state-of-the-art methods in standard test settings for image deconvolution.

Table I describes the different point spread functions (PSFs) and different variances of white Gaussian additive noise. We remark that these benchmark experiment settings are commonly used in many previous works [11][18].

TABLE I. EXPERIMENT SETTINGS WITH DIFFERENT BLUR KERNELS AND DIFFERENT VALUES OF NOISE VARIANCE σ^2 FOR PIXEL VALUES IN [0,255].

Scenario	PSF	σ^2
1	$1/(1+i^2+j^2)$, for $i, j = -7, \dots, 7$	2
2	$1/(1+i^2+j^2)$, for $i, j = -7, \dots, 7$	8
3	9×9 uniform kernel (boxcar)	≈ 0.3
4	$[1 \ 4 \ 6 \ 4 \ 1]^T [1 \ 4 \ 6 \ 4 \ 1]/256$	49
5	25×25 Gaussian with std = 1.6	4

In this section, the proposed GFD algorithm is compared with five currently state-of-the-art deconvolution algorithms, i.e., ForWaRD [4], APE-ADMM [33], L0-ABS [11], SURE-LET [12], and BM3DDEB [8]. The default parameters by the authors are applied for the developed algorithms. We emphasize that the APE-ADMM [33] is also an adaptive parameter selection method for total variance deconvolution. The comparison of our test results for different experiments against the other five methods in terms of ISNR are shown in Table II.

From Table II, we can see that our GFD algorithm achieves highly competitive performance and outperforms the other leading deconvolution algorithms in the most cases. The highest ISNR results in the experiments are labeled in bold.

One can see that ForWaRD method is less competitive for cartoon-like images than for these less structured images. The

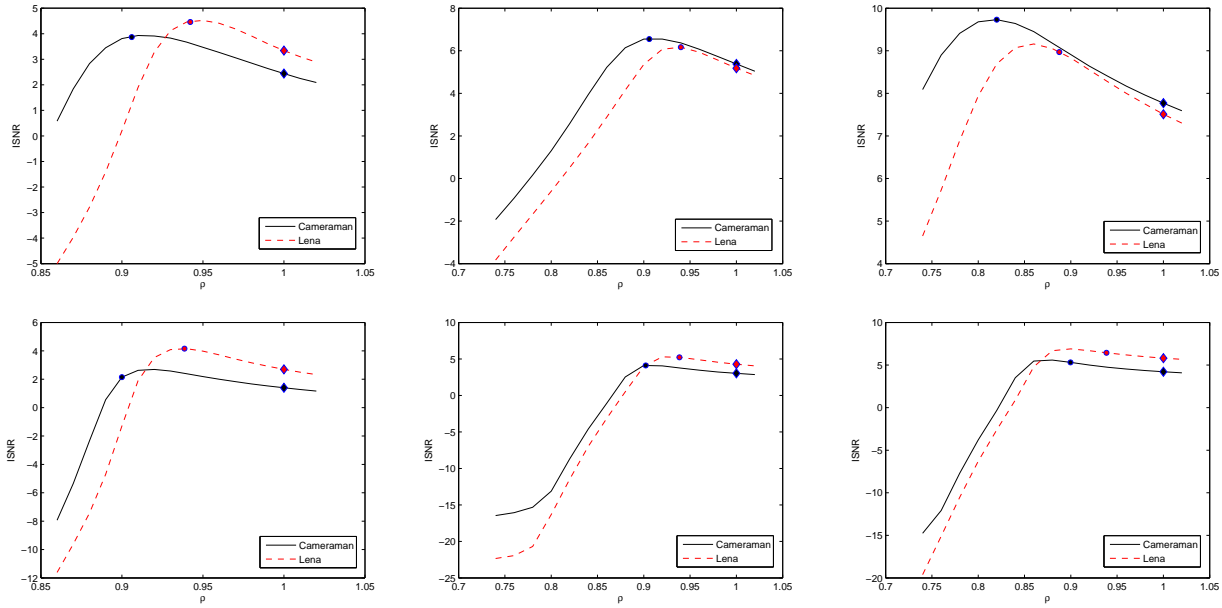


Fig. 3. Parameter ρ versus ISNR for *Cameraman* and *Lena* images. The images are blurred by a uniform blur of size 9×9 (first row) and a Gaussian blur of size 25×25 with variance 1.6 (second row). The ISNR values obtained by the proposed method and by $\rho = 1$ are marked by " \diamond " and " \bullet ", respectively.

TABLE II. COMPARISON OF THE OUTPUT ISNR(DB) OF THE PROPOSED DEBLURRING ALGORITHM. BSNR(BLURRED SIGNAL-TO-NOISE RATIO) IS DEFINED AS $BSNR = 10 \log_{10} Var(y)/N^2 \sigma^2$, WHERE $Var()$ IS THE VARIANCE.

	Scenario					Scenario				
Method	1	2	3	4	5	1	2	3	4	5
BSNR	31.87	25.85	40.00	18.53	29.19	29.16	23.14	40.00	15.99	26.61
ForWaRD	6.76	5.08	7.40	2.40	3.14	7.35	6.03	9.56	3.19	3.85
APE-ADMM	7.41	5.24	8.56	2.57	3.36	7.98	6.57	10.39	4.49	4.72
L0-Abs	7.70	5.55	9.10	2.93	3.49	8.40	7.12	11.06	4.55	4.80
SURE-LET	7.54	5.22	7.84	2.67	3.27	8.71	6.90	10.72	4.35	4.26
BM3DDEB	8.19	6.40	8.34	3.34	3.73	9.32	8.14	10.85	5.13	4.79
GFD	8.38	6.52	9.73	3.57	4.02	9.39	7.75	12.02	5.21	5.39
	Scenario					Scenario				
Method	1	2	3	4	5	1	2	3	4	5
BSNR	29.89	23.87	40.00	16.47	27.18	29.72	23.70	40.00	16.32	27.02
ForWaRD	6.05	4.90	6.97	2.93	3.50	5.15	3.87	6.47	2.19	2.71
APE-ADMM	6.36	4.98	7.87	3.52	3.61	5.82	4.28	7.14	2.58	2.98
L0-Abs	6.66	5.71	7.79	4.09	4.22	5.74	4.02	7.19	2.61	3.00
SURE-LET	7.71	5.88	7.96	4.42	4.25	6.01	4.32	6.89	2.75	3.01
BM3DDEB	7.95	6.53	8.06	4.81	4.37	6.34	4.81	6.99	3.05	3.22
GFD	8.12	6.65	8.97	4.77	4.95	6.29	4.83	7.67	3.11	3.50

TV model is substantially outperformed by our method for complicated images like *Cameraman* and *Man* with lots of disordered features and irregular edges, though it is well-known for its outstanding performance on regularly-structured images such as *Lena* and *House*.

SURE-LET and L0-ABS achieve higher average ISNR than ForWaRD and APE-ADMM, while our algorithm outperforms SURE-LET by 1.25 dB for scenario 3 and outperforms L0-ABS by 0.84 dB for the scenario 2, respectively. But L0-ABS cannot obtain top performance with all kinds of images and degradations without suitable for the image sparse representation and the mode parameters to the observed image. SURE-

LET approach is applicable for periodic boundary conditions, and can be used in various practical scenarios. But it also loses some details in the restored images.

BM3DDEB, which achieves the best performance on average, One can found that our method and BM3DDEB produce similar results, and achieve significant ISNR improvements over other leading methods. In average, our algorithm outperforms BM3DDEB by (0.095dB, -0.0325dB, 1.04dB, 0.0825dB, 0.46dB) for the five settings, respectively. In Figures 4~7, we show the visual comparisons of the deconvolution algorithms, from which it can be observed that the GFD approach produces sharper and cleaner image edges than other



Fig. 4. Visual quality comparison of image deblurring on gray image *Cameraman* (256×256). (a) original image, (b) noisy and blurred image (scenario 3), (c) the result of ForWaRD (ISNR=7.40dB), (d) the result of APE-ADMM (ISNR=8.56dB), (e) the result of L0-ABS (ISNR=9.10dB), (f) the result of SURE-LET (ISNR=7.84dB), (g) BM3DDEB result (ISNR = 8.34dB), and (h) the result of our method (ISNR = 9.73dB).

five methods.

From Figure 4, one can evaluate the visual quality of some restored images. It can be observed that our method is able to provides sharper image edges and suppress the ringing artifacts better than BM3DDEB. For *House* image (Figure 5), the differences between the various methods are clearly visible: our algorithm introduces fewer artifacts than the other methods. In Figure 6, our method achieves good preservation of regularly-sharp edges and uniform areas, while for *Man* image (Figure 7), it preserves the finer details of the irregularly-sharp edges.

In Figure 8, we plotted a few curves of different λ values versus iteration number, which were obtained from scenario 1 and 4 using *Cameraman* image, scenario 2 and 3 using *House* image, scenario 2 and 3 using *Lena* image, scenario 1 and 5 using *Man* image respectively. Hence, we emphasize that our approach automatically choose the regularization parameter at each iteration, unlike some of the other deconvolution algorithms such as [10], one has to manually tune the parameters, e.g., by running the method many times to choose the best one by error and trial.

C. Experiment 3 – Convergence

Since the guided image filter is highly nonlinear, it is difficult to prove the global convergence of our algorithm in theory. In this section, we only provide empirical evidence to show the stability of the proposed deconvolution algorithm.

In Figure 9, we show the convergence properties of the GFD algorithm for test images in the cases of scenario 5 (blur kernel is 25×25 Gaussian with $\text{std} = 1.6$, $\sigma = 2$) and scenario

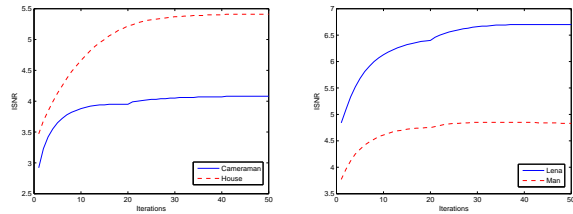


Fig. 9. Change of the ISNR with iterations for the different settings of the proposed algorithm. Left: deblurring of *Cameraman* and *House* images, scenario 5; Right: deblurring of *Lena* and *Man* images, scenario 2.

2 (PSF = $1/(1 + i^2 + j^2)$, for $i, j = -7, \dots, 7$, $\sigma = \sqrt{8}$) for four test images. One can see that all the ISNR curves grow monotonically with the increasing of iteration number, and finally become stable and flat. One can also found that 30 iterations are typically sufficient.

D. Analysis of Computational Complexity

In this work, all the experiments are performed in Matlab R2010b on a PC with Intel Core (TM) i5 CPU processor (3.30 GHz), 8.0G memory, and Windows 7 operating system.

In MATLAB simulation, we have obtained times per iteration of 0.057 seconds using 256×256 image, and about 30 iterations are enough.

The most computationally-intensive part of our algorithm is guided image filtering (3 times in one iteration). We mention that the guided filter can be simply sped up with subsampling,

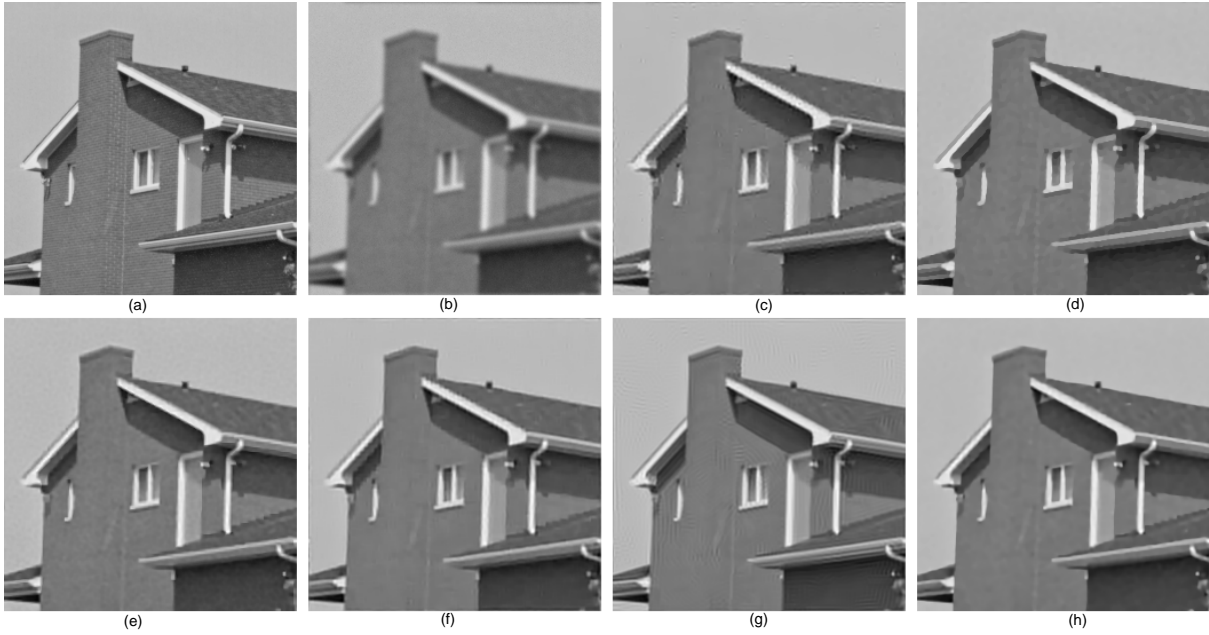


Fig. 5. Visual quality comparison of image deblurring on gray image *House* (256×256). (a) original image, (b) noisy and blurred image (scenario 5), (c) the result of ForWaRD (ISNR=3.85dB), (d) the result of APE-ADMM (ISNR=4.72dB), (e) the result of L0-ABS (ISNR=4.80dB), (f) the result of SURE-LET (ISNR=4.26dB), (g)BM3DDEB result (ISNR = 4.79dB), and (h) the result of our method (ISNR = 5.39dB).



Fig. 6. Details of the image deconvolution experiment on image *Lena* (512×512). (a) original image, (b) noisy and blurred image (scenario 1), (c) the result of ForWaRD (ISNR=6.05dB), (d) the result of APE-ADMM (ISNR=6.36dB), (e) the result of L0-ABS (ISNR=6.66dB), (f) the result of SURE-LET (ISNR=7.71dB), (g)BM3DDEB result (ISNR = 7.95dB), and (h) the result of our method (ISNR = 8.12dB).

and this will lead to a speedup of 10 times with almost no visible degradation[41].

V. CONCLUSION

We have developed an image deconvolution algorithm based on an explicit image filter : guided filter, which has been



Fig. 7. Details of the image deconvolution experiment on image *Man* (512×512). (a) original image, (b) noisy and blurred image (scenario 3), (c) the result of ForWaRD (ISNR=6.47dB), (d) the result of APE-ADMM (ISNR=7.14dB), (e) the result of L0-ABS (ISNR=7.19dB), (f) the result of SURE-LET (ISNR=6.89dB), (g) BM3DDEB result (ISNR = 6.99dB), and (h) the result of our method (ISNR = 7.67dB).

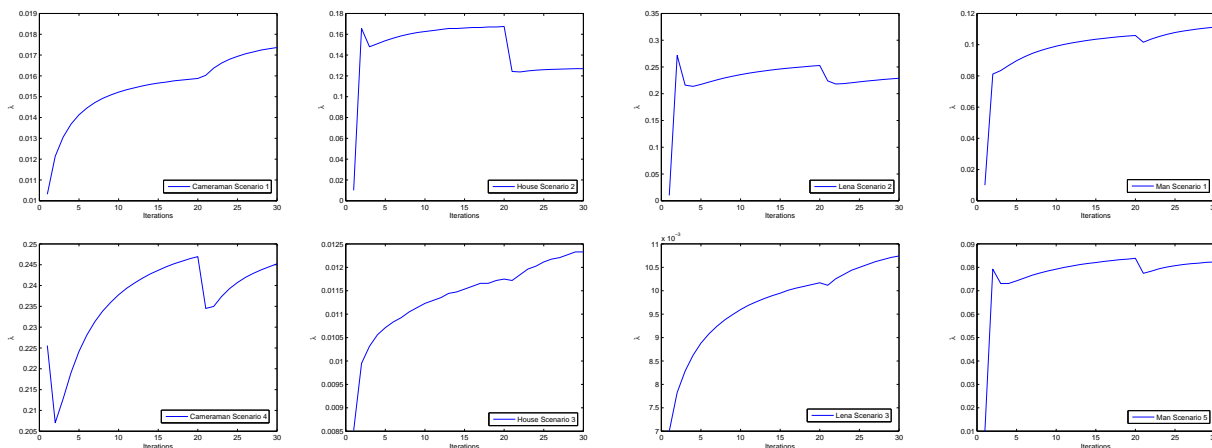


Fig. 8. Regularization parameter versus iterations number. The *Cameraman* image is tested by Scenario 1 and 4; The *House* image is tested by Scenario 2 and 3; The *Lena* image is tested by Scenario 2 and 3; The *Man* image is tested by Scenario 1 and 5.

proved to be more effective than the bilateral filter in several applications. We first introduce guided filter into the image restoration problem and propose an efficient method, which obtains high quality results. The simulation results show that our method outperforms some existing competitive deconvolution method. We find remarkable how such a simple method compares to other much more sophisticated methods. Based on Morozov’s discrepancy principle, we also propose a simple but effective method to automatically determine the regularization parameter at each iteration.

REFERENCES

- [1] P. C. Hansen. *Rank-Deficient and Discrete Ill-Posed Problems: Numerical Aspects of Linear Inversion*. Philadelphia, PA: SIAM, 1998.
- [2] L. Sun, S. Cho, J. Wang, and J.Hays, "Good Image Priors for Non-blind Deconvolution: Generic vs Specific", In *Proc. of the European Conference on Computer Vision (ECCV)*, pp.231-246, 2014.
- [3] C. Schuler, H.Burger, S.Harmeling, and B. Scholkopf,"A machine learning approach for non-blind image deconvolution", In *Proc. of Int. Conf. Comput. Vision and Pattern Recognition (CVPR)*, pp.1067-1074., 2013.
- [4] R.Neelamani, H.Choi, and R.G.Baraniuk, "ForWaRD: Fourier-wavelet

- regularized deconvolution for ill-conditioned systems," *IEEE Trans. Signal Process.*, vol.52, pp.418-433, Feb. 2004.
- [5] Hang Yang, Zhongbo Zhang, "Fusion of Wave Atom-based Wiener Shrinkage Filter and Joint Non-local Means Filter for Texture-Preserving Image Deconvolution" *Optical Engineering.*, vol.51, no.6, 67-75, (Jun. 2012).
- [6] J. A. Guerrero-Colon, L. Mancera, and J. Portilla. "Image restoration using space-variant Gaussian scale mixtures in overcomplete pyramids." *IEEE Trans. Image Process.*, vol.17, no.1, pp.27-41, 2007.
- [7] A. Foi, K.Dabov, V.Katkovnik, and K.Egiazarian. "Shape-adaptive DCT for denoising and image reconstruction." In *Soc. Photo-Optical Instrumentation Engineers*, vol 6064, pp 203-214, 2006.
- [8] K. Dabov, A.Foi, V.Katkovnik, and K.Egiazarian. "Image restoration by sparse 3D transform-domain collaborative filtering." In *Soc. Photo-Optical Instrumentation Engineers*, vol 6812, pp 6, 2008.
- [9] L. Rudin, S. Osher, and E. Fatemi. "Nonlinear total variation based noise removal algorithms." *Physica D*, vol.60, pp.259-268, 1992.
- [10] Y. Wang, J. Yang, W. Yin, and Y. Zhang, "A new alternating minimization algorithm for total variation image reconstruction," *SIAM J.Imag. Sci.*, vol.1, pp.248-272, 2008.
- [11] J. Portilla. "Image restoration through l0 analysis-based sparse optimization in tight frames." In *IEEE Int. Conf Image Processing (ICIP)*, pp.3909-3912. 2009.
- [12] F. Xue, F.Luisier, and T.Blu. "Multi-Wiener SURE-LET Deconvolution." *IEEE Trans. Image Process.*, vol.22, no.5, pp.1954-1968, 2013.
- [13] O.V. Michailovich. "An Iterative Shrinkage Approach to Total-Variation Image Restoration." *IEEE Trans. Image Process.*, vol.20, no.5, pp.1281-1299, 2011.
- [14] M. Ng, P. Weiss, and X. Yuan, "Solving constrained total-variation image restoration and reconstruction problems via alternating direction methods," *SIAM J. Sci. Comput.*,vol.32, pp.2710-2736, Aug. 2010.
- [15] Hang Yang, Ming Zhu, Zhongbo Zhang, Heyan Huang, "Guided Filter based Edge-preserving Image Non-blind Deconvolution", In *Proc. 20th IEEE International Conference on Image Processing (ICIP)*, Oral, Melbourne, Australia, 2013.
- [16] Hang Yang, Zhongbo Zhang, Ming Zhu, Heyan Huang, "Edge-preserving image deconvolution with nonlocal domain transform", *Optics and Laser Technology*, vol.54, pp.128-136, 2013.
- [17] W. Dong, L. Zhang, G. Shi, and X. Wu. "Image deblurring and super-resolution by adaptive sparse domain selection and adaptive regularization." *IEEE Trans. Image Process.*, vol.20, no.7, pp.1838-1857, 2011.
- [18] W. Dong, L. Zhang, G. Shi, and X. Li. Nonlocally centralized sparse representation for image restoration. *IEEE Trans. Image Process.*, vol.22, no.4, pp.1620-1630, 2013.
- [19] J. Mairal, F. Bach, J. Ponce, G. Sapiro, and A. Zisserman. Non-local sparse models for image restoration. In *IEEE Int. Conf. Comput. Vision*, pp. 2272-2279. IEEE, 2009.
- [20] J.Zhang, D.Zhao, W.Gao, "Group-based sparse representation for image restoration," *IEEE Transactions on Image Processing*, vol.23 ,no.8, pp.3336-3351, 2014.
- [21] K. Dabov, A.Foi, V. Katkovnik, and K. Egiazarian. "Image restoration by sparse 3D transform-domain collaborative filtering." *Proc SPIE Electronic Image'08*. vol.6812, San Jose, 2008.
- [22] R. Rubinstein, A. M. Bruckstein, and M. Elad, "Dictionaries for sparse representation modeling," *Proc. IEEE*, vol.98, pp.1045-1057, Jun. 2010.
- [23] W. Dong, G. Shi, and X. Li. "Nonlocal image restoration with bilateral variance estimation: A low-rank approach," *IEEE Trans. Image Process.*, vol.22, no.2, pp.700-711, 2013.
- [24] H. Ji, C. Liu, Z. Shen, and Y. Xu. "Robust video denoising using low rank matrix completion". In *IEEE Int. Conf. Comput. Vision and Pattern Recognition*, pp. 1791-1798, 2010.
- [25] H. Yang, G.S. Hu, Y. Q. Wang and X.T.Wu. "Low-Rank Approach for Image Non-blind Deconvolution with Variance Estimation." *SPIE Journal of Eletronic Imaging*, vol.24, no.6, pp.1122-1142, 2015.
- [26] T. Goldstein and S. Osher, "The split Bregman method for L1-regularized problems," *SIAM J. Imag. Sci.*, vol. 2, no. 2, pp. 323C343,2009.
- [27] C. Wu and X.-C. Tai, "Augmented Lagrangian method, dual methods, and split Bregman iteration for ROF, vectorial TV, and high order models," *SIAM J. Imag. Sci.*, vol. 3, no. 3, pp. 300C339, 2010.
- [28] P. C. Hansen, "Analysis of discrete ill-posed problems by means of the L-curve," *SIAM Rev.*, vol. 34, no. 4, pp. 561-580, 1992.
- [29] J. M. Bioucas-Dias, M. A. T. Figueiredo, and J. P. Oliveira, "Adaptive total variation image deblurring: A majorization-minimization approach," in *Proc. EUSIPCO, Florence, Italy*, 2006.
- [30] H. Liao, F. Li, and M. K. Ng, "Selection of regularization parameter in total variation image restoration," *J. Opt. Soc. Amer. A, Opt., Image Sci., Vis.*, vol. 26, no. 11, pp. 2311C2320, Nov. 2009.
- [31] S. D. Babacan, R. Molina, and A. K. Katsaggelos, "Parameter estimation in TV image restoration using variational distribution approximation," *IEEE Trans. Image Process.*, vol. 17, no. 3, pp. 326-339, Mar. 2008
- [32] Y. W. Wen and R. H. Chan, "Parameter selection for total-variation based image restoration using discrepancy principle," *IEEE Trans. Image Process.*, vol. 21, no. 4, pp. 1770C1781, Apr. 2012.
- [33] C. He, C. Hu, W. Zhang, and B. Shi, "A Fast Adaptive Parameter Estimation for Total Variation Image Restoration", *IEEE Trans. Image Process.*, vol. 23, no. 12, pp. 4954C4967, Dec. 2014.
- [34] S. Li, X. Kang, and J. Hu, "Image Fusion with Guided Filtering", *IEEE Trans. Image Process.*, vol. 22, no. 7, pp. 2864-2875, Mar. 2013
- [35] C. Tomasi, and R. Manduchi. "Bilateral filtering for gray and color images." In *IEEE Int. Conf. Comput. Vision*, pp. 839-846. IEEE, 1998.
- [36] L. Xu, C. Lu, Y. Xu, and J. Jia. "Image smoothing via L0 gradient minimization." In *ACM Trans. Graphics* vol. 30, pp. 174. ACM, 2011.
- [37] K. He, J. Sun, X. Tang. "Guided image filtering". In *Proc. of the European Conference on Computer Vision*, vol.1, pp.1-14, 2010.
- [38] K. He, J. Sun, X. Tang, "Guided Image Filtering", *IEEE Transactions on Pattern Analysis and Machine Intelligence*, vol.35, no.6, pp.1397-1409, 2013.
- [39] S. Anzengruber and R. Ramlau, "Morozov's discrepancy principle for Tikhonov-type functionals with non-linear operators," *Inverse Problems*, vol.26, pp.1-17, 2010.
- [40] S. Mallat, *A Wavelet Tour of Signal Processing*, 2nd ed. San Diego, CA, USA: Academic, 1999
- [41] K. He, J. Sun, "Fast Guided Filter." arXiv preprint arXiv:1505.00996, 2015.